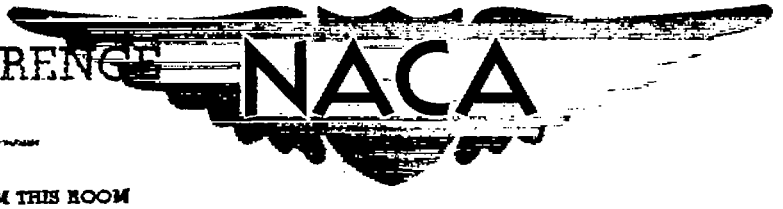

RESEARCH MEMORANDUM

EXPERIMENTAL AND THEORETICAL INVESTIGATION OF ROTATING-STALL CHARACTERISTICS OF SINGLE-STAGE AXIAL-FLOW COMPRESSOR WITH HUB-TIP RATIO OF 0.76

By Robert W. Graham and Vasily D. Prian

Lewis Flight Propulsion Laboratory
Cleveland, Ohio

NATIONAL ADVISORY COMMITTEE
FOR AERONAUTICS

WASHINGTON
November 30, 1953

NACA RM E53I09

NATIONAL ADVISORY COMMITTEE FOR AERONAUTICS

RESEARCH MEMORANDUM

EXPERIMENTAL AND THEORETICAL INVESTIGATION OF ROTATING-STALL CHARACTERISTICS OF SINGLE-STAGE AXIAL-FLOW COMPRESSOR WITH HUB-TIP RATIO OF 0.76

By Robert W. Graham and Vasily D. Prian

SUMMARY

The over-all performance and the rotating-stall characteristics of a single-stage compressor with a hub-tip ratio of 0.76 and a symmetrical velocity diagram were investigated over a wide range of weight flow for 60, 70, 80, and 100 percent of design speed. No discontinuities in the performance characteristic were observed at any operating condition. Rotating-stall patterns were observed that extended radially over the entire blade span (total-span rotating stall) and over a part of the blade span in the tip region (partial-span rotating stall). The number of total-span stall zones varied from two to four, whereas the number of partial-span rotating stall zones varied from three to eight. The partial-span stall zones rotated at 0.25 rotor speed and the total-span stall zones at 0.49 rotor speed, both rotating in the same direction as the rotor with respect to an absolute coordinate reference.

Compressor speed did not appear to influence the magnitude of the flow coefficients marking the boundaries of the partial-span and total-span rotating-stall regions on the compressor performance map. However, hysteresis effects shifted the rotating-stall regions to higher values of flow coefficient for increasing weight flow than the flow coefficients for decreasing weight flow.

A theory on rotating stall was applied to the rotating-stall data of the compressor described herein and other single-stage, symmetrical design compressors in an attempt to evaluate some of the factors that affect the mechanism of rotating stall. For both partial-span and total-span rotating stalls, a single correlation was obtained between a stall-propagation-rate parameter and the aerodynamic phase angle of the rotor blades. The terms "partial-span" and "total-span" rotating stall are descriptive of the radial extent of the stall zones and do not denote two unique types of stall propagation.

INTRODUCTION

It has been observed that, in general, the blade rows of axial-flow compressors do not stall uniformly around the annulus but that stall zones develop that rotate tangentially within the annulus. These low-flow zones rotate at a lower speed than the rotor and usually in the direction of the rotor rotation with respect to an absolute reference. As a flow fluctuation, rotating stall is of current interest because of its effect on the aerodynamic performance of compressors and its potential destructive effect on axial-flow-compressor blading. Reference 1 contains a discussion of this effect of rotating stall on blade vibrations.

In reference 2, a theoretical study suggested that flow patterns without axial symmetry can exist in an axial-flow compressor within the region of blade stall when the lift coefficient - angle of attack relation exhibits nonlinearity or hysteresis. In reference 3, the hysteresis in the lift characteristic of an airfoil is attributed to a lag between the established velocity distribution over the airfoil and the aerodynamic restoring forces that maintain the velocity distribution in equilibrium.

Reference 4 shows that rotating stalls observed experimentally may be described according to the radial extent of the stall region into the flow passage. A stall region may extend across the entire span of the blade or only over a part of the blade. In this report, stall across the entire blade span will be referred to as a total-span rotating stall; and that over part of the blade, as a partial-span rotating stall.

The purpose of the present investigation was to study the rotating stall associated with the performance of a typical middle stage of a multistage compressor designed with a symmetrical velocity diagram at all radii. The rotating-stall data obtained from this compressor stage are compared with stall data obtained from other compressors of symmetrical design in an effort to develop a greater understanding of the fundamental factors affecting rotating-stall propagation.

SYMBOLS

The following symbols are used in this report:

b $\quad \tan \alpha = \dfrac{\text{Relative tangential stall velocity}}{\text{Axial velocity}}$ (fig. 2(b))

C_L coefficient of lift

c_p specific heat at constant pressure, Btu/(lb)($^\circ$F)

g	acceleration due to gravity, 32.17 ft/sec/sec
h	dimensionless ratio of axial component of air velocity to rotor tip speed
J	mechanical equivalent of heat, 778.3 ft-lb/Btu
k	ratio of rotor tangential velocity relative to stall to absolute axial velocity component
m	slope or lift curve with respect to angle of attack
P	total pressure, lb/sq ft
T	total temperature, $^{\circ}R$
U	wheel speed, ft/sec
V	absolute air velocity, ft/sec
V'	relative air velocity, ft/sec
X	ratio of circumferential component of absolute velocity of entering air to rotor tip speed
Y	ratio of change in circumferential component of velocity to rotor tip speed
Z	ratio of blade-element velocity to rotor tip speed
α	angle of initial swirl relative to rotating-stall pattern, deg (fig. 2(b))
β	absolute air angle, deg (fig. 2(a))
β'	relative air angle, deg (fig. 2(a))
γ	ratio of specific heats
Δ	phase angle or lag of aerodynamic restoring forces
η	adiabatic efficiency
λ	number of rotating stalls
ν	ratio of stall-propagation rate relative to rotor with respect to rotor speed

[redacted]

ρ density of air, lb/cu ft

σ solidity, ratio of chord length to spacing

Φ flow coefficient, V_z/U_m

Subscripts:

ac actual

m evaluated at mean radius

t evaluated at tip radius

z axial component

1 after guide vanes

2 after stator

3 compressor exit

Barred symbol indicates average value.

APPARATUS

Test Facility

A schematic diagram of the compressor installation is shown in figure 1. Air from the test cell was drawn through the thin-plate orifice at the entrance to the orifice tank and then through a motor-operated butterfly inlet valve into the depression tank. After passing through a paper filter and a honeycomb in the depression tank, the air entered the compressor through a bellmouth inlet section. The air was discharged from the compressor into the laboratory exhaust system. A motor-operated butterfly valve in the exhaust line was used to control the air flow through the compressor. A high-speed a-c dynamometer drove the compressor; speed control of the dynamometer was achieved by frequency regulation of a variable frequency unit that supplied electric power to the dynamometer.

Compressor Stage

The compressor stage consisted of 35 guide vanes, 37 rotor blades, and 39 stator blades. The tip diameter was 14 inches, and the hub-tip ratio measured at the entrance to the rotor row was 0.76, a representative value for the middle stage of multistage compressors.

The design of the rotor and stator blade rows was based upon a symmetrical velocity diagram at all radii and approximately constant total enthalpy at each blade element. The axial velocity distribution before and after the blade row was calculated with a simplified radial equilibrium relation that neglected radial entropy variations and the radial accelerations of the air flow and considered only the equilibrium between the radial pressure forces and the centrifugal fluid forces. In the aerodynamic design analysis, the maximum relative Mach number was restricted to a value less than 0.7, and the blade-loading parameter $C_L\sigma$ was restricted to a value of 0.9. A detailed description of the procedure employed in designing the compressor stage appears in reference 5. Cascade data on the performance of NACA series 65 airfoils that appeared graphically in reference 5 were employed in selecting the blade profile. The design data for the compressor stage are presented in figure 2.

The constant-thickness, circular-arc, sheet-metal guide vanes were set at zero angle of inlet incidence. The guide vanes were designed by the design method described in reference 6, in which secondary flow effects are considered in calculating the blade-element turning of the guide vanes.

INSTRUMENTATION

Over-All Performance

The over-all performance of the stage was determined from measurements of total temperature and total pressure at the depression tank and at the compressor exit approximately $2\frac{1}{4}$ inches downstream of the trailing edge of the stator blades. At the compressor exit, the pressure and temperature measurements were made at the area centers of five equal annular areas. Two 15-tube circumferential pressure rakes and two 3-tip circumferential thermocouple rakes were used in the radial surveys (fig. 3(a)). The thermocouple probe was designed with a flow-direction claw that made possible the orientation of the probe in the flow direction.

Detection of Rotating Stalls

Hot-wire-anemometer instrumentation similar to that described in reference 7 was employed to detect the rotating-stall patterns and to measure the amplitude of the flow fluctuations within the stall regions. In order to obtain sufficient data to determine the number of stall zones, two hot-wire anemometers were located in approximately the same axial plane after the stator row. The included angle between the two

probes was varied from 60° to 120° in increments of 30°, so that the number of stall zones could be computed from the phase shift in the observed stall-pattern trace obtained from each hot-wire probe. Data from one angle setting are usually insufficient to determine a unique result for the number of stall zones present; for example, a four- and an eight-stall-zone pattern will appear identical for a 90°-probe-angle setting.

The tungsten anemometer wires were 0.0002 inch in diameter and 0.08 inch long. Two types of anemometer probe were used: for one type, the wire was mounted perpendicular to the axis of the probe (fig. 3(b)), and for the other, the wire was mounted parallel to the probe (fig. 3(c)). The parallel-wire type did not have to be rotated to accommodate changes in the flow direction; whereas the perpendicular wire was better suited for determining the radial depth of the stall region, despite its sensitivity to flow-angle changes. The voltage drop across the hot wire, which was dependent upon the air flow, was amplified and fed into a dual-beam cathode-ray oscilloscope. A common sweep generator triggered both beams so that the phase difference between the stall traces of each probe could be indicated. The phase-difference data were used in calculating the number of stall regions. A photographic record was taken of the stall patterns appearing on the oscilloscope screen. Typical stall-pattern photographs are shown in figure 4.

An audio-frequency oscillator was used in conjunction with the oscilloscope to determine the frequency with which the stall regions passed one of the anemometer probes.

The anemometer wires were susceptible to frequent breakage caused by oil or dirt particles in the air stream. It was observed that wire life was longer when the wire was situated near the outer casing wall. Consequently, radial surveys with the hot wires were made as rapidly as possible, and the wires were kept near the casing wall during most of the stall investigation.

PROCEDURE AND METHOD OF CALCULATION

The over-all performance of the compressor stage was investigated at corrected tip speeds of 498, 568, 640, 710, and 790 feet per second, which correspond to 60, 70, 80, 90, and 100 percent of design speed, respectively. At each of these speeds, the air flow was varied from the maximum obtainable to a minimum value at which the outlet throttle was almost entirely closed.

The total pressure after the stage was calculated from an arithmetic average of the total-pressure readings obtained during a radial survey. The total pressure at the inlet to the rotor was calculated by

correcting the depression-tank pressure readings for the total-pressure loss due to the guide vanes. The total-temperature rise across the stage was obtained by arithmetically averaging the total-temperature readings. As was pointed out in the section on instrumentation, the five radial stations used in the radial surveys of temperature and pressure were area centers of equal areas. Therefore, the averaged values of temperature rise across the stage and total pressure after the stage are area-weighted averages.

The adiabatic efficiency of the stage is defined as the ratio of the calculated isentropic work to the actual work:

$$\eta = \frac{gJc_pT_1\left[\left(\frac{P_3}{P_1}\right)_{ac}^{\frac{\gamma-1}{\gamma}} - 1\right]}{gJc_p(T_3 - T_1)} \qquad (1)$$

After the over-all stage performance data were obtained, hot-wire anemometers were employed to investigate the stall patterns behind the rotor for the following speeds: 60, 70, 80, and 100 percent of design speed. The 90-percent design-speed investigation was omitted, because dynamometer speed regulation was difficult at that speed. The stall patterns were observed for both increasing and decreasing weight flow, during which sufficient performance data were obtained to locate each stall pattern on the performance map of the stage. With the calculation procedure of reference 8, the number of rotating stalls λ was determined from data obtained from the photographic records of the stall patterns that appeared on the oscilloscope screen. The flow fluctuations within the stall region were calculated by the procedure presented in references 7 and 8. The flow fluctuations are presented in terms of a dimensionless parameter $\Delta\rho V/\overline{\rho V}$.

RESULTS AND DISCUSSION

Over-All Performance

A performance map of the compressor stage described herein is given in figure 5. The maximum adiabatic efficiency, which was approximately 85 percent, occurred at design speed and at a flow coefficient of 0.65. The peak-efficiency points for all the constant-speed curves occurred within a narrow band of flow coefficient ranging from 0.65 to 0.75, and the magnitude of the peak efficiencies diminished with the compressor speed. A maximum total-pressure ratio across the stage of 1.245 was achieved at design-speed operation. No perceptible discontinuities in the performance curves were observed for the regions in which rotating stall was present. Severe performance discontinuities attributable to the presence of rotating stall were reported in reference 1.

[redacted]

Types of Rotating Stall Observed

The types of rotating stall observed were similar to those observed by other investigators, namely a stall region that extended over the entire span of the blade (total-span rotating stall) and a stall region that extended over a portion of the blade span (partial-span rotating stall).

The stall patterns observed are shown schematically superposed on the compressor performance map in figure 6. Table I summarizes the pertinent data of the rotating-stall patterns. Each rotating-stall region shown in figure 6 is identified according to the number of stall zones present and the flow-coefficient range over which the stall pattern prevails for accelerating and decelerating flow. For decelerating flow, blade stall as evidenced by stall wakes was first observed at an approximate flow coefficient of 0.62. Further reductions of the flow coefficient increased the severity of the separation of flow from the individual blades. As the flow coefficient approached a value of 0.52, nonperiodic stall zones covering several blade passages were observed. In figure 6 this region of blade stall is labeled "Region of transition A." At the higher compressor speeds, partial-span rotating stalls were evident at a flow coefficient of 0.52 when the weight flow was decreased. No partial-span stalls were apparent at the lower compressor speeds; the region of transition A appeared to extend into the flow-coefficient region where partial-span rotating stall at the rotor tip was observed at the higher compressor speeds. The periodic partial-span rotating stalls disappeared below a flow coefficient of 0.45. For the higher compressor speeds, another region of transition (region of transition B, fig. 6) occurred in which the compressor blades were either partially or completely stalled along the blade span, but no periodic rotating-stall zones were apparent. The total-span rotating-stall region was observed at all compressor speeds, beginning at a flow coefficient of 0.34 as the weight flow was diminished.

As is evident from table I, the ratio of stall rotational speed to compressor speed was 0.25 and remained nearly constant over the entire partial-span stall region, regardless of the number of stalls and the compressor speed. The magnitude of the ratio of stall rotational speed to compressor speed for the partial-span stall is somewhat lower than values previously reported in the literature for similar compressor designs, for which the aforementioned ratio varied from 0.40 to 0.80 (ref. 4). Table I shows that the number of stall zones within the partial-span stall region varied from three to eight, which is similar to the spread of values reported in reference 4. In reference 1 the number of partial-span stall zones increased in numerical sequence as the flow coefficient diminished, whereas examination of figure 6 reveals that the formation of different stall patterns in this case did not always follow a numerical sequence as the weight flow or flow coefficient was decreased.

The ratio of stall rotational speed to compressor speed for total-span rotating stall remained at a value close to 0.49 within the entire total-span rotating-stall region (see table I). A comparison of this value with values appearing in the literature (0.30 to 0.40) reveals a similarity in magnitude. However, the number of stall zones observed is greater than the number observed in investigations of similarly designed stages. According to figure 6, the number of total-span stall zones diminished as the weight flow was reduced.

Circumferential Extent of Stall Zones

The circumferential width of the stall zones was estimated from the photographs of the stall traces. Figure 7 shows schematic diagrams of the distribution of the stall zones around the annulus of the compressor. For either partial-span or total-span stall zones, the percentage of the tip circumference occupied by the stall zones remained essentially constant for each compressor speed and independent of the number of the stall zones present. Consequently, the circumferential extent of the individual stall zones increased when the number of stall zones around the annulus decreased at a given compressor speed.

Flow Fluctuations Incited by Rotating Stall

The fluid velocity fluctuation parameter $\Delta\rho V/\overline{\rho V}$ is a ratio of the fluid momentum fluctuations to the mean or average fluid momentum. Table I presents computed values of $\Delta\rho V/\overline{\rho V}$ for the stall patterns observed that are of the same general magnitude as those reported in reference 1.

Rotating-Stall Hysteresis

Examination of figure 6 reveals that rotating stall was incited at approximately the same flow coefficient for all compressor speeds. This coincidence of the flow coefficients indicates that the instigation of rotating stall is independent of the compressor speed. For a two-dimensional model of the flow through a compressor stage, the instigation of rotating stall may be considered to be related to the angle of attack (which depends on the flow coefficient), provided the geometry of the compressor stage remains unchanged. The flow coefficients marking the inception of rotating stall were greater in magnitude for accelerating flow than for decelerating flow. This apparent shift in the rotating-stall regions to higher flow-coefficient values for accelerating flow as compared with decelerating flow is attributed to a hysteresis effect. The aerodynamic conditions that cause the establishment of rotating stall apparently lag the flow coefficient similarly to the manner in

which the flux density lags the magnetic force to cause the familiar magnetic hysteresis. These aerodynamic conditions are not yet well understood.

Theoretical Results

A description of a theory on rotating stall is presented in reference 9. The basic assumptions underlying this theoretical analysis are:

(1) The rotor blades can be represented by a vortex sheet or actuator sheet that is referred to a frame of reference that rotates at the same speed as the asymmetric flow. The flow is considered to be steady with respect to the frame of reference.

(2) The circulation distribution, which results from induced velocity effects of the asymmetric-flow blade loading, sustains the induced velocity effects.

(3) The asymmetric-flow disturbances can be represented as small perturbations.

These assumptions were applied to two types of analysis. In the first analysis the compressor blades were considered to be airfoil sections, and in the second analysis "channel relations" obtained from cascade tests completed by W. D. Rannie were employed. Analytical solutions representing steadily rotating asymmetric flow were obtained when the compressor blades were considered to be stalled and a phase angle Δ (representing the phase lag between the variation of the lift with the angle of attack) was introduced into the analysis.

The rotating-stall data reported herein and additional rotating-stall data from references 1 and 8 were utilized in an analysis involving the aerodynamic-theory approach presented in reference 9. The pertinent equations and a discussion of the analytical procedure involving the previously mentioned rotating-stall data are presented in appendix A. It should be emphasized that the rotating-stall data were obtained from tests conducted with several single-stage compressors that were designed with a symmetrical velocity diagram at the pitch radius, and no other type of compressor design was incorporated in the analysis. Both partial-span and total-span rotating stalls were included in the data.

Figure 8 presents a family of curves representing constant values of phase angle Δ. The ordinate is a ratio of the rotor blade velocity relative to the rotating-stall speed to the axial air velocity, and the abscissa is the tangent of the relative inlet-air angle. Figure 8 is similar to figure 5 of reference 9; the solid-line curves of constant phase angle Δ in figure 8 were obtained from the reference. The data

points for each constant speed of rotating stall lie along curves of approximately constant phase angle. Furthermore, a plot of Δ as a function of the observed stall-propagation rate relative to the rotor (fig. 9) shows that the phase angle diminishes as the stall speed relative to the rotor increases.

The extrapolation of the curve in figure 9 indicates that the relative stall speed is equal in magnitude to the rotor speed when the phase angle is zero. The direction of the rotating-stall propagation relative to the rotor is in the opposite direction to the rotor rotation. Consequently, when the stall-propagation rate is equal to the rotor speed, the net absolute stall velocity is zero. When such a condition exists, the stall zone (or zones) can be thought of as being fixed in the compressor annulus, and no phase lag exists between lift and angle of attack.

The right side of equation (A4) becomes infinite when Δ equals zero. Consequently, Δ must equal 90° to satisfy the equation, and thus the curve in figure 9 can be extrapolated to pass through the point where ν equals zero and Δ equals 90°. If this condition would actually exist physically, the stall zones would rotate at zero velocity relative to the rotor.

Figure 9 indicates that there is a correlation between the phase angle Δ and the rotating-stall-propagation rate. Whether the rotating-stall pattern is partial-span or total-span does not appear to influence the correlation. This suggests that the terms "partial-span" and "total-span" classify rotating stalls according to the size or extent of the stall zone only and do not denote two kinds of rotating stall that have distinctive propagation mechanisms.

Examination of equation (A4) in appendix A reveals that the phase angle Δ is related to the flow coefficient Φ and the absolute air inlet angle β as well as to the stall-propagation parameter ν. However, from figure 9 it appears that Δ and ν are the principal variables that influence the relation (eq. (A4)). The minor importance of β and Φ should be examined. For the compressor stages considered in the analysis, the magnitude of β can be considered to be a constant (22°). Phase angle Δ is plotted as a function of Φ with ν as a parameter in figure 10, where data from the various stall patterns employed in the analysis are shown. This figure indicates that the magnitude of Δ remains substantially constant over the range of Φ in which a given type of rotating-stall pattern occurs. For the rotating-stall data incorporated in figure 9, β and Φ are noninfluential; thus the phase angle and the stall-propagation rate are interdependent.

In reference 3, it was assumed that the phase angle is a function of the slope of the curve of lift plotted against angle of attack. Sears

(ref. 9) made the same assumptions for his airfoil analysis and developed a relation between the slope of the lift curve and the average velocity diagram at the mean radius, the geometry of the blade row, the phase angle, and the stall-propagation rate. This relation expressed in terms of dimensionless parameters used in this report is equation (B4) of appendix B. The curves in figure 11 represent solutions of equation (B4) for constant values of ν and β; the points represent experimental data. The values of Δ were obtained from figure 9. The slope of the lift curve in the rotating-stall region appears to be related to the phase angle Δ, as well as to the flow coefficient and the compressor geometry.

Conclusions of Theoretical Analysis

The rotating-stall data employed in the theoretical correlation presented herein were limited to single-stage compressors designed with a symmetrical velocity diagram at the pitch radius. Other types of compressor design need to be investigated as to their rotating-stall characteristics in order to evaluate the influence of compressor design variables on a theoretical correlation involving rotating-stall-propagation rates. Perhaps, from an accummulation of rotating-stall data for several types of compressor design, it will be possible in the design procedure to predict the propagation rate and the number of stall zones of a rotating stall peculiar to a compressor stage.

SUMMARY OF RESULTS

Experimental

From the investigation of the over-all performance and rotating-stall characteristics of a single-stage axial-flow compressor with a hub-tip ratio of 0.76, the following results were obtained:

1. At design tip speed, the maximum adiabatic efficiency obtained was 0.85 at a flow coefficient of 0.650, and the maximum total-pressure ratio was 1.245 at a flow coefficient of 0.625. No perceptible discontinuities in the performance curves were observed for the regions in which rotating stall was present.

2. Rotating stalls that extended radially over a portion of the blade chord (partial-span) and over the entire blade chord (total-span) were observed. Both types of stall rotated in the direction of the rotor rotation as measured from an absolute frame of reference; the partial-span rotated at 0.25 rotor speed and the total-span at 0.49 rotor speed.

3. The number of stall zones ranged from two to four for the total-span and from three to eight for the partial-span stalls. Within the total-span region, the number of stall zones diminished as the flow coefficient diminished; whereas within the partial-span region, no similar trend was apparent. The partial-span stall zones were apparent at 80-percent design speed and at design speed, but not at the lower operating speeds. Blade stall was present at the lower speeds for the range of flow coefficient corresponding to partial-span rotating stall at 80- and 100-percent design speed; however, no periodic rotating-stall zones were observed.

4. The circumferential extent of the partial-span stalls ranged from 37 to 100 percent of the tip circumference, and the total-span stalls extended over 38 to 58 percent of the tip circumference. The percentage of the tip circumference occupied by the stall zones remained approximately constant for each compressor speed and appeared independent of the number of stall zones present.

5. The coincidence of the flow coefficients corresponding to the instigation of rotating stall for all compressor speeds indicated that the instigation of rotating stall is independent of the compressor speed. Hysteresis effects caused the magnitude of the flow coefficients marking the inception of rotating stall to be greater for accelerating flow than for decelerating flow.

Theoretical

A theory on rotating stall originated by W. R. Sears of Cornell University was employed in a theoretical analysis involving rotating-stall data from several single-stage, symmetrical-design, axial-flow compressors, including the stage reported herein. The results of the theoretical analysis are as follows:

6. A correlation exists between the stall-propagation rate in symmetrical-design single-stage compressors and the aerodynamic phase angle between lift and angle of attack. The correlation is independent of the type of rotating stall (partial- or total-span).

7. The angle of attack corresponding to the inception of a rotating-stall pattern seems to be related to the aerodynamic phase angle as well as to the flow coefficient and the geometry of the single-stage compressor.

Lewis Flight Propulsion Laboratory
National Advisory Committee for Aeronautics
Cleveland, Ohio, September 3, 1953

APPENDIX A

COMPUTATION OF MEAN-RADIUS RELATIVE INLET-AIR ANGLE AND PHASE ANGLE Δ

The abscissa of figure 8 is the tangent of the relative inlet-air angle. Experimental values of this angle were not available for the single-stage symmetrical-design compressors that had been investigated for rotating-stall patterns. For the purposes of the analysis involving the equations of reference 9, only the relative inlet-air angle at the mean radius was considered. The following simplifying assumptions were made in calculating the mean relative inlet-air angle:

(1) The turning angle of the inlet guide vanes remained constant at all weight flows.

(2) The flow coefficient was evaluated at the mean blade radius with the use of the stage entrance conditions.

The following relations were employed in the computations:

From definitions based on reference (9):

$$\tan \beta' = k + b = \frac{1}{\Phi} - \tan \beta \tag{a}$$

$$k = \frac{\nu}{\Phi} \tag{b}$$

$$b = \frac{1}{\Phi}(1 - \Phi \tan \beta - \nu) \tag{c}$$

The parameter b is also defined as

$$b = \tan \alpha \tag{d}$$

Consequently,

$$\sin \alpha = \frac{b}{\sqrt{1+b^2}} \tag{e}$$

$$\cos \alpha = \frac{1}{\sqrt{1+b^2}} \tag{f}$$

From reference 9 (eq. (33))

$$\tan \Delta = \frac{k^2 \sin \alpha \cos \alpha + 2k + b}{k^2 \cos^2 \alpha} \tag{A1}$$

[redacted]

Substituting definitions (b), (e), and (f) in equation (A1) and rearranging give

$$\tan \Delta = b + \frac{2\Phi}{\nu}(1+b^2) + \frac{(1+b^2)b\Phi^2}{\nu^2} \tag{A2}$$

Substituting definition (c) in equation (A2) yields

$$\tan \Delta = \frac{1}{\Phi}(1 - \Phi \tan \beta - \nu) + \frac{2\Phi}{\nu}\left[1 + \frac{1}{\Phi^2}(1 - \Phi \tan \beta - \nu)^2\right] + \frac{\Phi^2}{\nu^2}\left[1 + \frac{1}{\Phi^2}(1 - \Phi \tan \beta - \nu)^2\right]\left(\frac{1 - \Phi \tan \beta - \nu}{\Phi}\right) \tag{A3}$$

Rearranging equation (A3) gives

$$\tan \Delta = \frac{1}{\Phi}(1 - \Phi \tan \beta - \nu) + \left[1 + \frac{1}{\Phi^2}(1 - \Phi \tan \beta - \nu)^2\right]\left[\frac{\Phi}{\nu^2}(1 - \Phi \tan \beta + \nu)\right] \tag{A4}$$

[redacted]

APPENDIX B

DERIVATION OF EXPRESSION FOR SLOPE OF LIFT CURVE

From reference 9, the equation for the slope of the lift curve is

$$m = \frac{-4\sqrt{1 + (b+k)^2}}{k^2 \cos^2 \alpha} \frac{\cos \Delta}{\sigma} \tag{B1}$$

Rewriting equation (B1) so as to include the definitions in appendix A gives

$$m = \frac{-4\sqrt{1 + \tan^2 \beta'}}{\left(\frac{\nu}{\Phi}\right)^2 \frac{1}{1 + \left(\tan \beta' - \frac{\nu}{\Phi}\right)^2}} \frac{\cos \Delta}{\sigma} \tag{B2}$$

From the velocity triangle in figure 2, it is evident that the tangent of the relative inlet-air angle can be expressed as

$$\tan \beta' = \frac{U_m}{V_z} - \Phi \frac{U_m}{V_z} \tan \beta = \frac{1}{\Phi} (1 - \Phi \tan \beta) \tag{B3}$$

The mean-radius absolute inlet-air angle β is the flow angle leaving the guide vanes, is approximately constant for all symmetrical designs, and is independent of the flow coefficient.

Substitution of equation (B3) into equation (B2) results in

$$m = \frac{-4\sqrt{1 + \frac{1}{\Phi^2}\left(1 - \Phi \tan \beta\right)^2} \frac{\cos \Delta}{\sigma}}{\frac{\nu^2}{\Phi^2 + (1 - \nu - \Phi \tan \beta)^2}} \tag{B4}$$

REFERENCES

1. Huppert, Merle C., Johnson, Donald F., and Costilow, Eleanor L.: Preliminary Investigation of Compressor Blade Vibration Excited by Rotating Stall. NACA RM E52J15, 1952.

2. Sears, W. R.: On Asymmetric Flow in an Axial-Flow Compressor Stage. Paper No. 52-F-15, presented at meeting of A.S.M.E., Chicago (Ill.), Sept. 8-11, 1952.

3. Mendelson, Alexander: Effect of Aerodynamic Hysteresis on Critical Flutter Speed at Stall. NACA RM E8B04, 1948.

4. Huppert Merle C., and Benser, William A.: Some Stall and Surge Phenomena in Axial-Flow Compressors. Paper presented at Twenty-First Inst. Aero. Sci. meeting, New York (N.Y.), Jan. 26-29, 1953.

5. Johnsen, Irving A.: Investigation of a 10-Stage Subsonic Axial-Flow Research Compressor. I - Aerodynamic Design. NACA RM E52B18, 1952.

6. Lieblein, Seymour: Turning-Angle Design Rules for Constant-Thickness Circular-Arc Inlet Guide Vanes in Axial Annular Flow. NACA TN 2179, 1950.

7. Laurence, James C., and Landes, L. Gene: Auxiliary Equipment and Techniques for Adapting the Constant-Temperature Hot-Wire Anemometer to Specific Problems in Air-Flow Measurements. NACA TN 2843, 1952.

8. Huppert, Merle C.: Preliminary Investigation of Flow Fluctuations During Surge and Blade Row Stall in Axial-Flow Compressors. NACA RM E52E28, 1952.

9. Sears, W. R.: A Theory of "Rotating Stall" in Axial Flow Compressors. Graduate School Aero. Eng., Cornell Univ., Ithaca (N.Y.). (Contract No. AF 33 (038)-21406.)

TABLE I. - SUMMARY OF STALL PATTERNS

Type of stall	Compressor speed, percent design	Lissajous frequency, cps	Number of stalls, λ	Stall frequency, cps	Ratio of stall speed to rotor speed, absolute, $1 - \nu$	Ratio of stall speed to rotor speed, relative, ν	Fluctuation parameter, $\Delta\rho V/\overline{\rho V}$
Total[a]	60	202	3	67.4	0.48	0.52	1.73
	70	228	3	76.1	0.47	0.53	
		305	4	76.8	.47	.53	1.40
	80	175	2	87.5	0.49	0.51	1.43
		260	3	86.8	.49	.51	
		343	4	85.7	.48	.52	1.21
	100	210	2	105	0.48	0.52	1.72
		325	3	108	.49	.51	1.55
		440	4	110	.49	.51	1.40
Partial[b]	80	220	5	45	0.25	0.75	1.54
		310	7	44.5	.25	.75	1.31
		350	8	44.0	.25	.75	1.15
	100	158	3	52	0.23	0.77	2.02
		268	5	53.6	.24	.76	
		368	7	52.5	.24	.76	
		400	8	50	.23	.77	1.63

[a]Total-span rotating stall.

[b]Partial-span rotating stall.

[redacted]

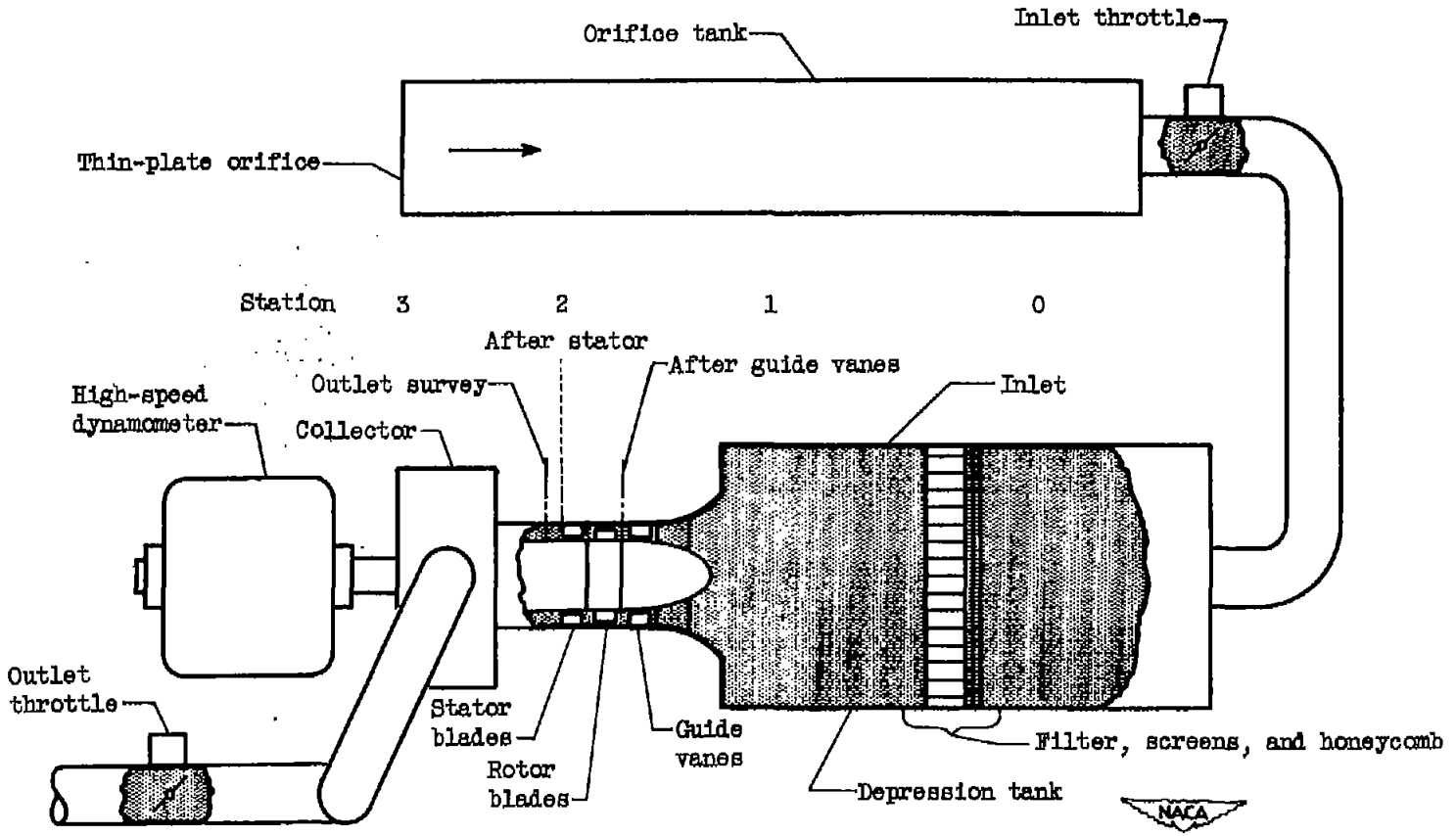

Figure 1. - Schematic diagram of compressor installation.

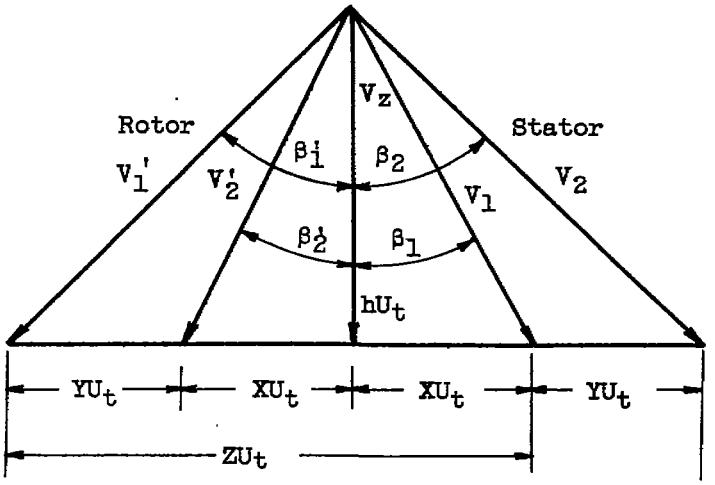

Z	X	Y	h	V/U_t	β', deg	$C_L\sigma$	σ	Angle of attack, deg
Rotor								
0.7639	0.1899	0.3842	0.7636	0.9554	36.94	0.8673	1.064	17.33
.8230	.2332	.3566	.7471	.9518	38.29	.8169	.988	15.69
.8820	.2746	.3328	.7267	.9471	39.89	.7750	.922	14.28
.9410	.3146	.3119	.7024	.9412	41.37	.7399	.864	12.91
1.000	.3533	.2935	.6737	.9340	43.83	.7109	.813	11.49
Z	X	Y	h	V/U_t	β	$C_L\sigma$	σ	Angle of attack, deg
Stator								
0.7838	0.1903	0.3888	0.8212	1.0050	35.19	0.8744	1.093	15.37
.8379	.2304	.3637	.7817	.9818	37.23	.8289	1.022	14.61
.8919	.2688	.3417	.7389	.9585	39.56	.7904	.960	14.22
.9460	.3060	.3221	.6920	.9346	42.23	.7577	.906	13.96
1.000	.3420	.3047	.6404	.9101	45.28	.7302	.857	13.85

(a) Symmetrical axial velocity diagram and design data for compressor stage.

Figure 2. - Velocity diagrams and design data.

2987

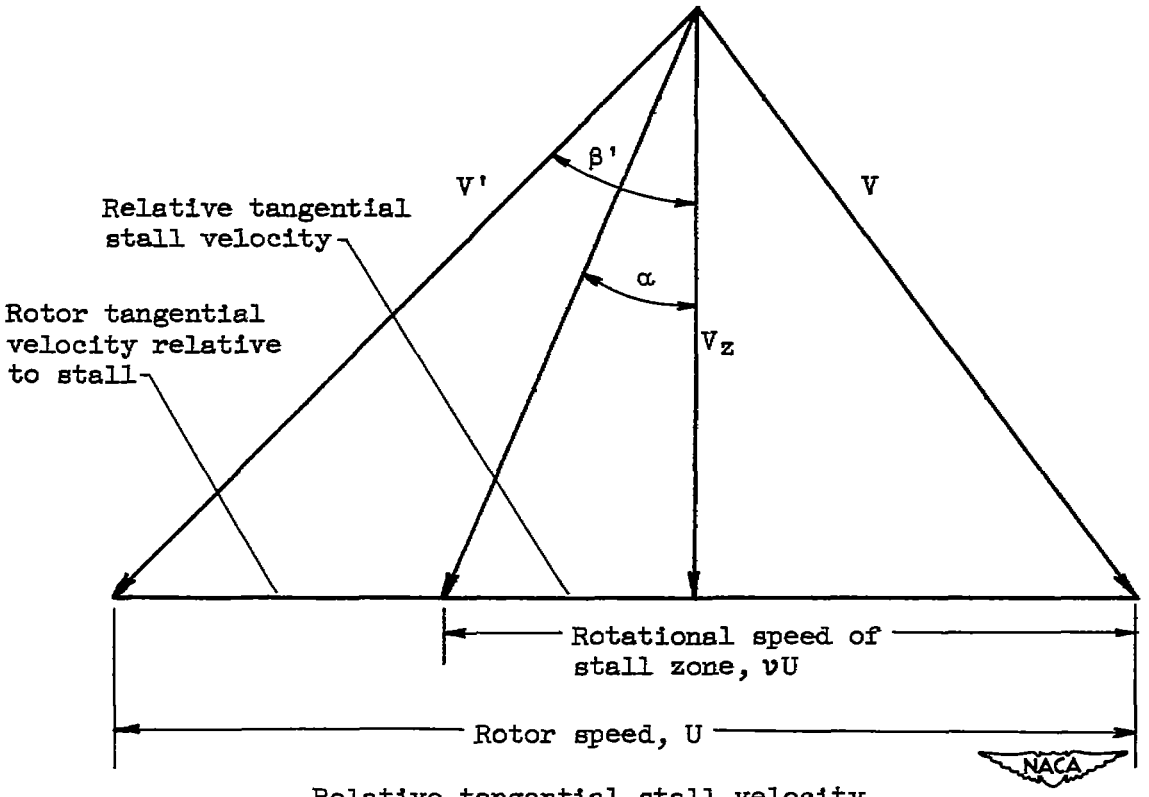

$$b = \frac{\text{Relative tangential stall velocity}}{V_z}$$

$$k = \frac{\text{Rotor tangential velocity relative to stall}}{V_z}$$

(b) Velocity diagram defining swirl angle α.

Figure 2. - Concluded. Velocity diagrams and design data.

[redacted]

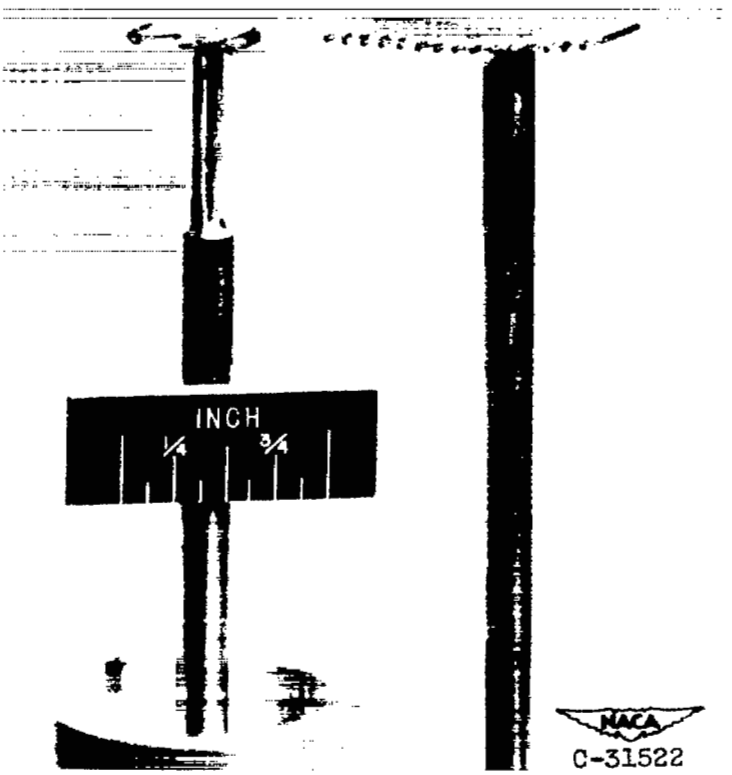

(a) Discharge total-temperature and -pressure rakes.

Figure 3. - Instrumentation.

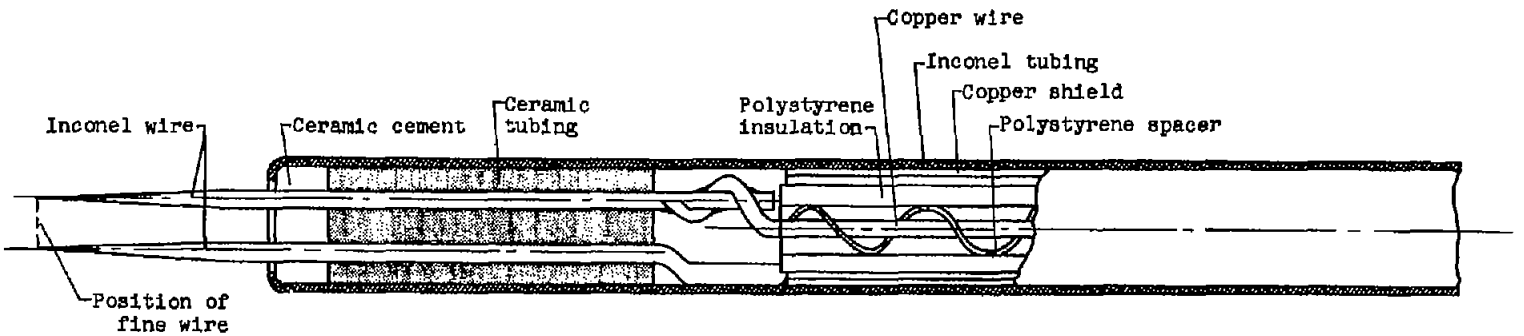

(b) Anemometer 1. Wire mounted perpendicular to probe axis; low-temperature probe.

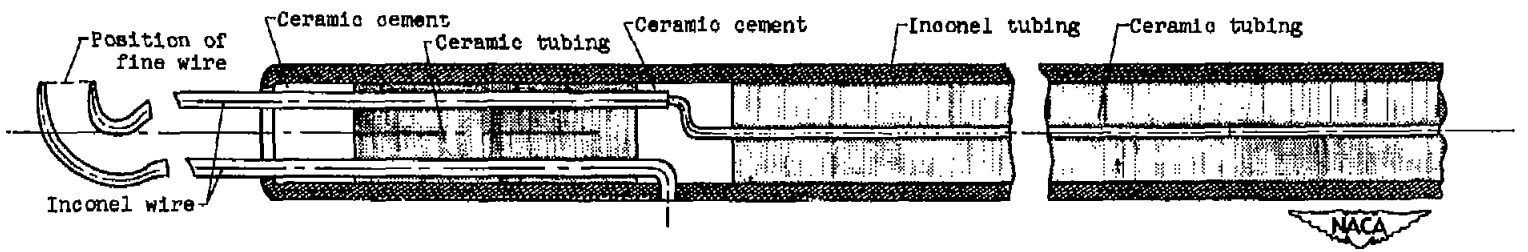

(c) Anemometer 2. Wire mounted parallel to probe axis; high-temperature probe.

Figure 3. - Concluded. Instrumentation.

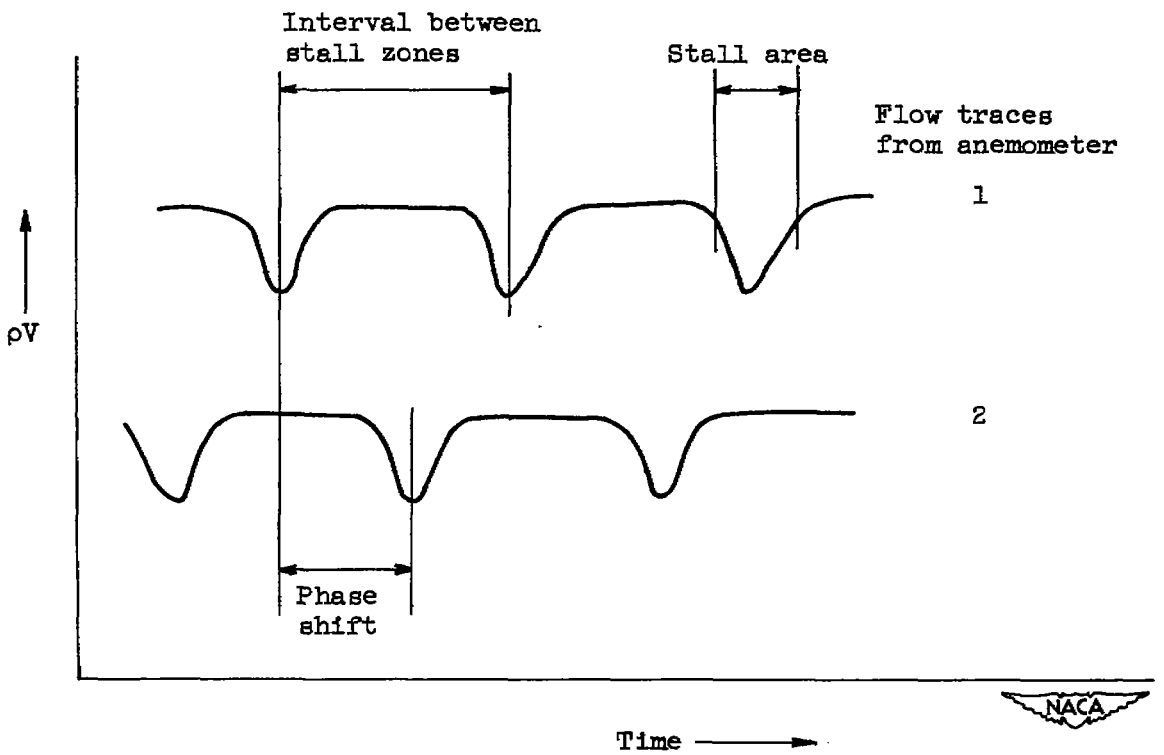

(a) Oscillogram sketched from cathode-ray oscilloscope.

Figure 4. - Typical stall patterns observed on cathode-ray oscilloscope.

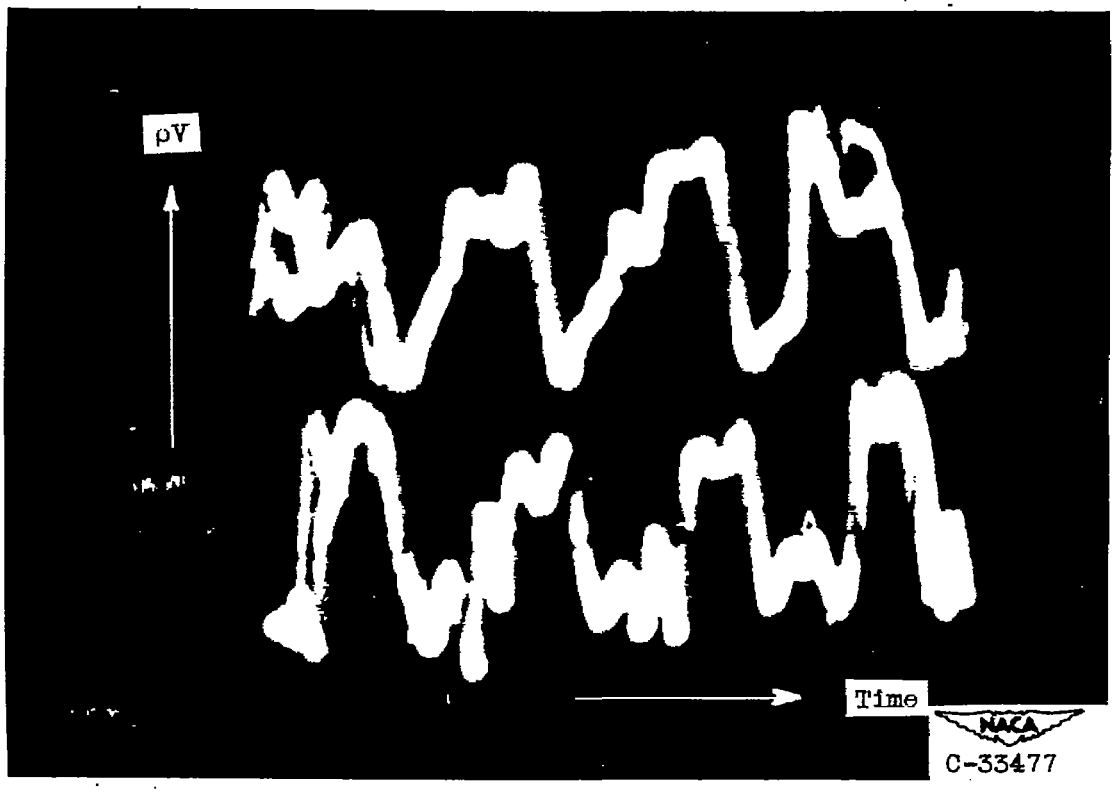

(b) Number of stalls, 3; frequency, 325 cycles per second; total-span stall, 100 percent of design; flow coefficient, 0.338; radius-tip position; accelerating flow; $\Delta\rho V/\overline{\rho V} = 1.550$.

Figure 4. - Continued. Typical stall patterns observed on cathode-ray oscilloscope.

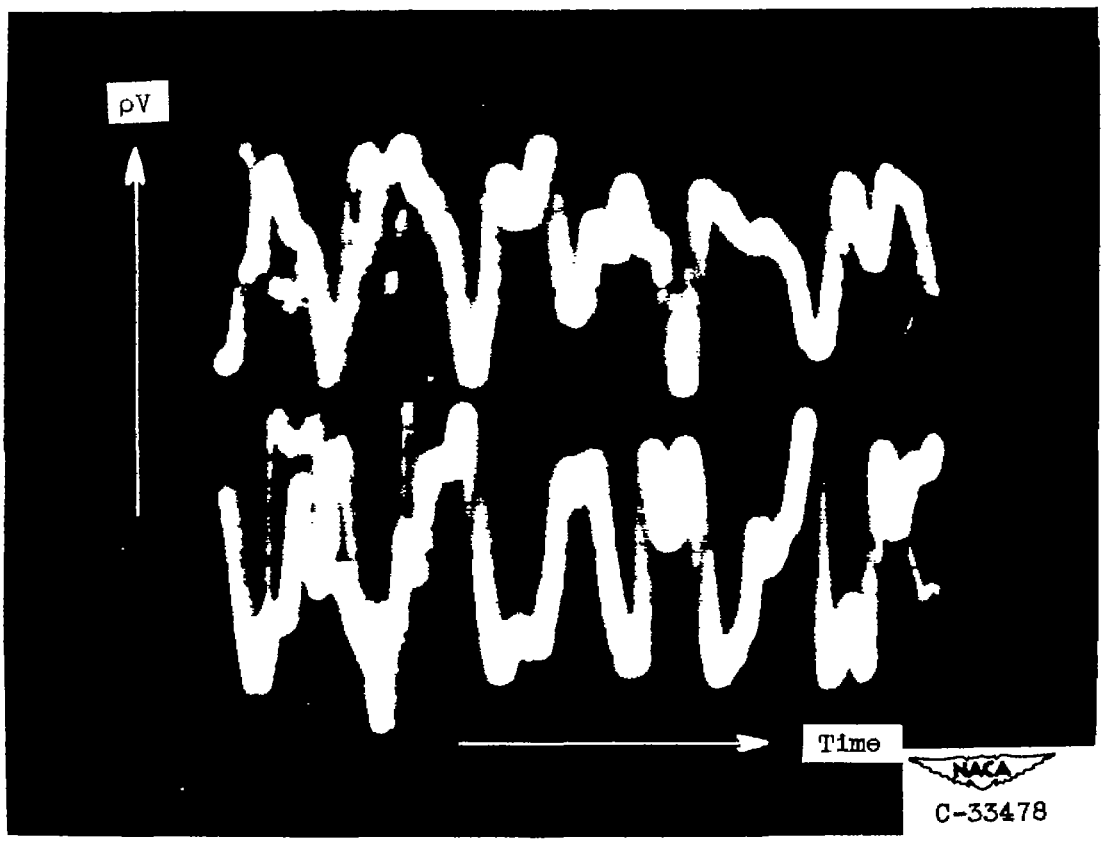

(c) Number of stalls, 4; frequency, 440 cycles per second; total-span stall, 100 percent of design; flow coefficient, 0.321; radius-tip position; decelerating flow; $\Delta\rho V/\rho V = 1.400$.

Figure 4. - Concluded. Typical stall patterns observed on cathode-ray oscilloscope.

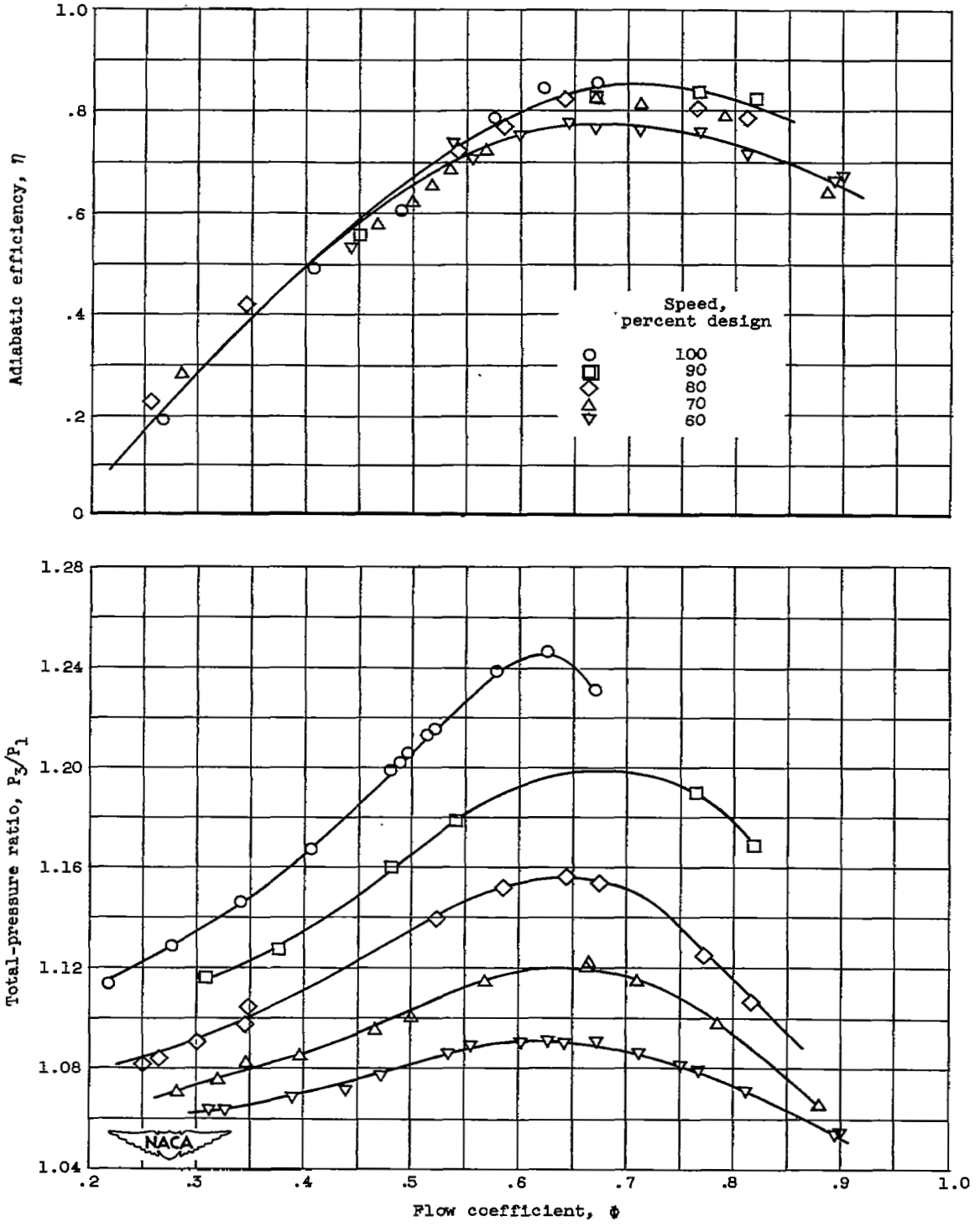

Figure 5. - Performance map.

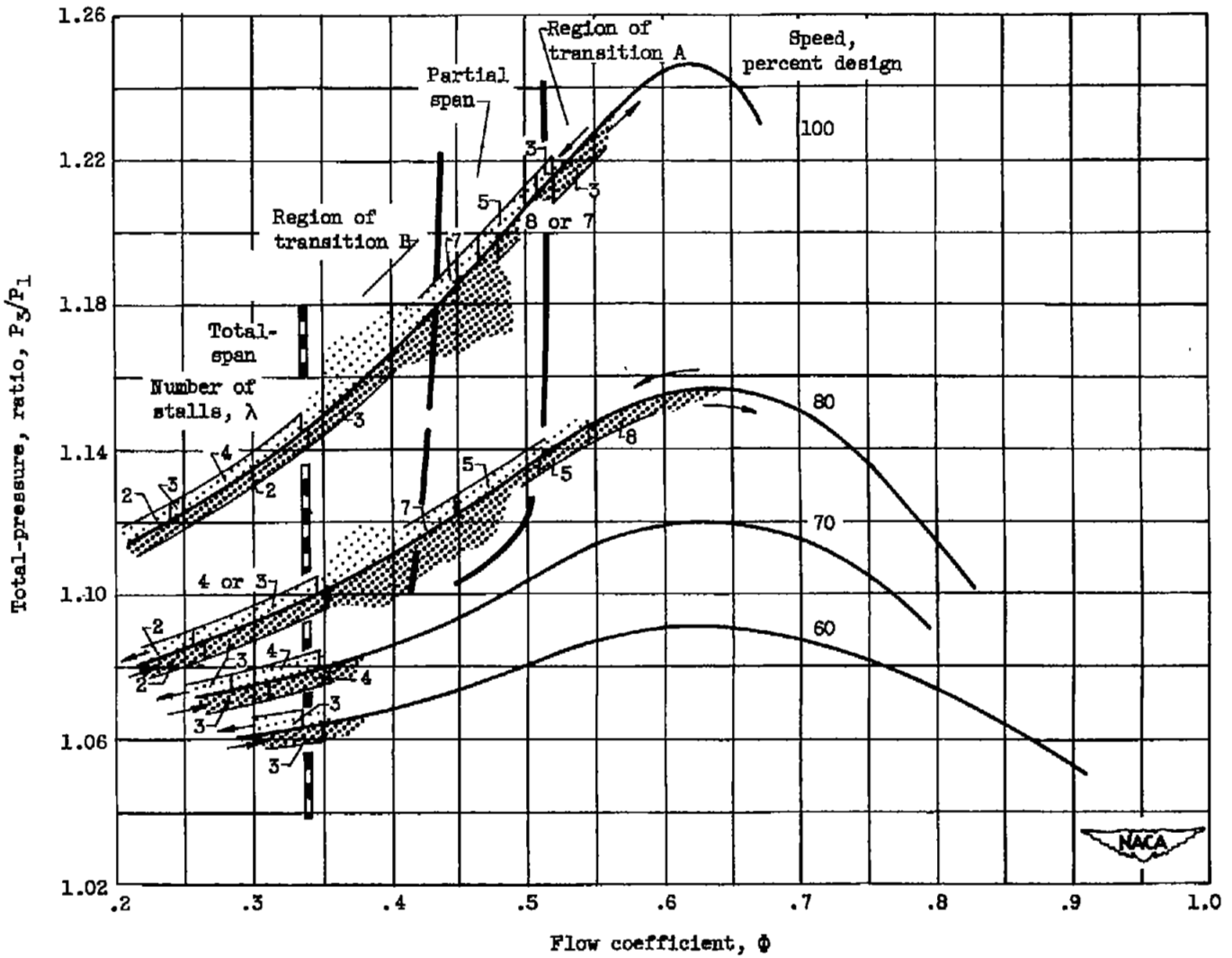

Figure 6. - Observed rotating-stall patterns.

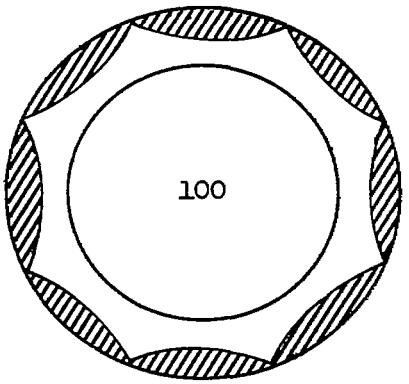

Stall zones, 8
Tip circumference occupied,
100 percent

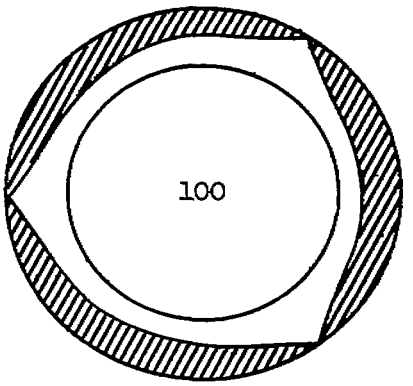

Stall zones, 3
Tip circumference occupied,
100 percent

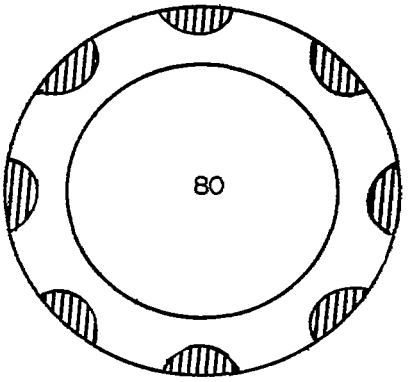

Stall zones, 8
Tip circumference occupied,
44 percent

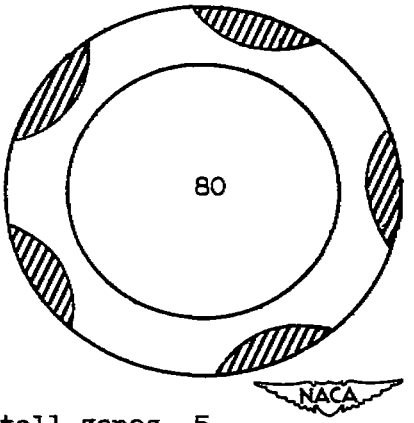

Stall zones, 5
Tip circumference occupied,
37 percent

(a) Partial-span rotating stall.

Figure 7. - Circumferential extent of stall zones. Figures in centers represent percentage of design speed.

[redacted]

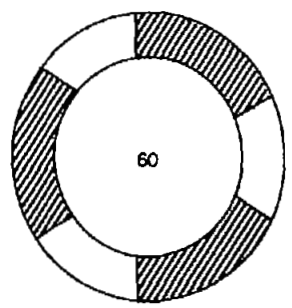

Stall zones, 3
Tip circumference occupied,
58 percent

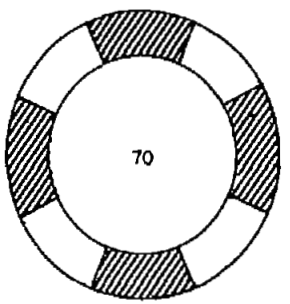

Stall zones, 4
Tip circumference occupied,
56 percent

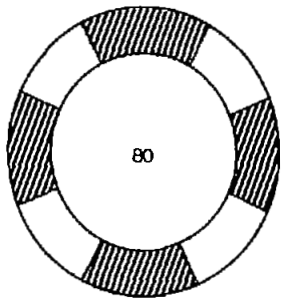

Stall zones, 4
Tip circumference occupied,
56 percent

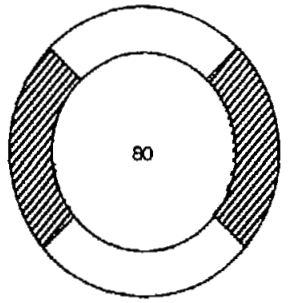

Stall zones, 2
Tip circumference occupied,
50 percent

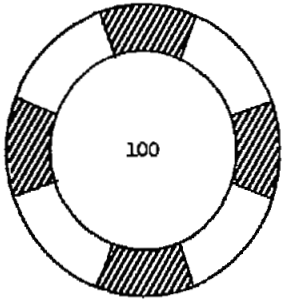

Stall zones, 4
Tip circumference occupied,
38 percent

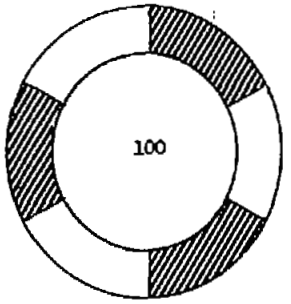

Stall zones, 3
Tip circumference occupied,
41 percent

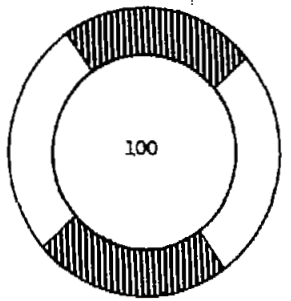

Stall zones, 2
Tip circumference occupied,
38 percent

NACA

(b) Total-span rotating stall.

Figure 7. - Concluded. Circumferential extent of stall zones. Figures in centers represent percentage of design speed.

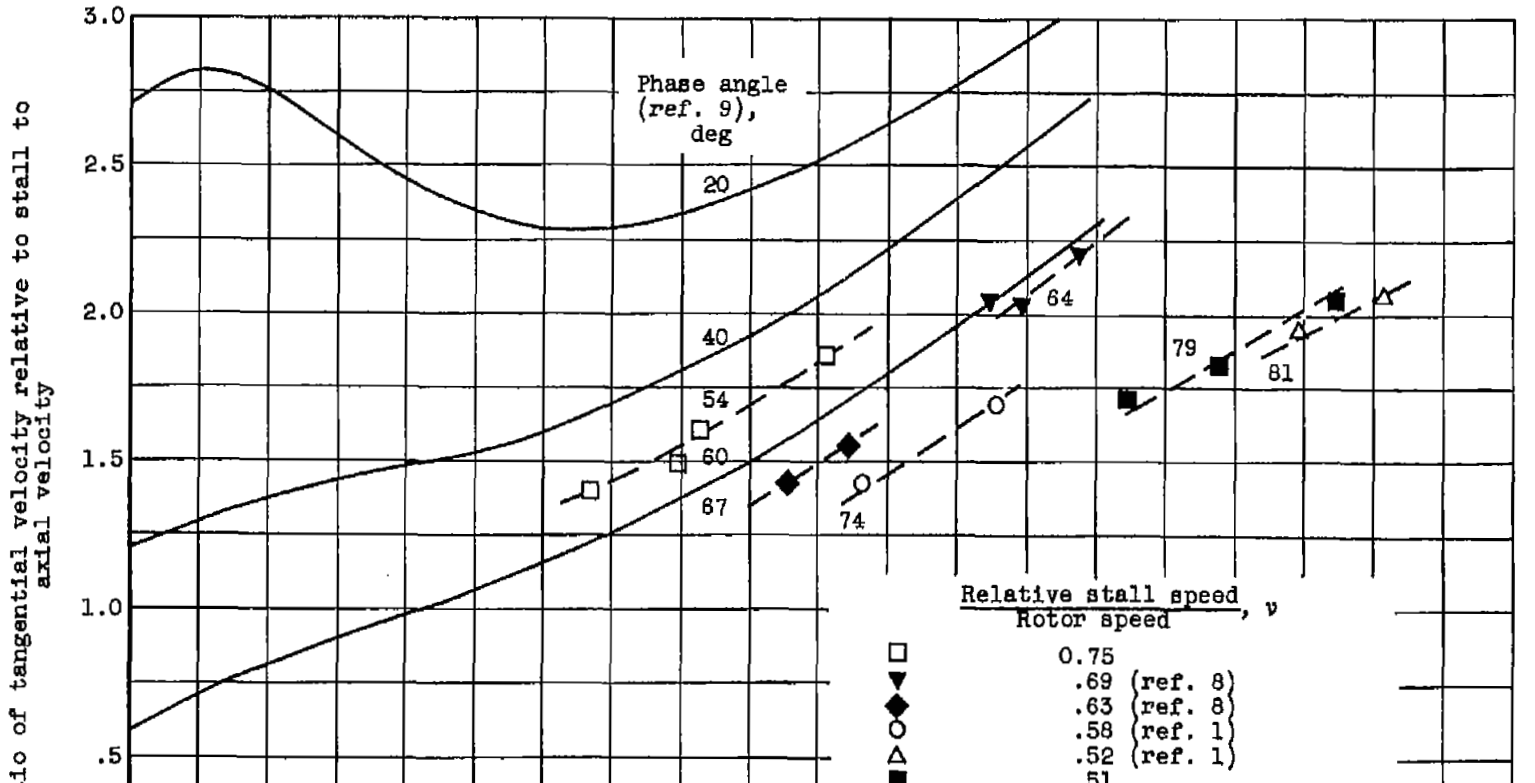

Figure 8. - Correlation of stall data with analytically derived phase angle.

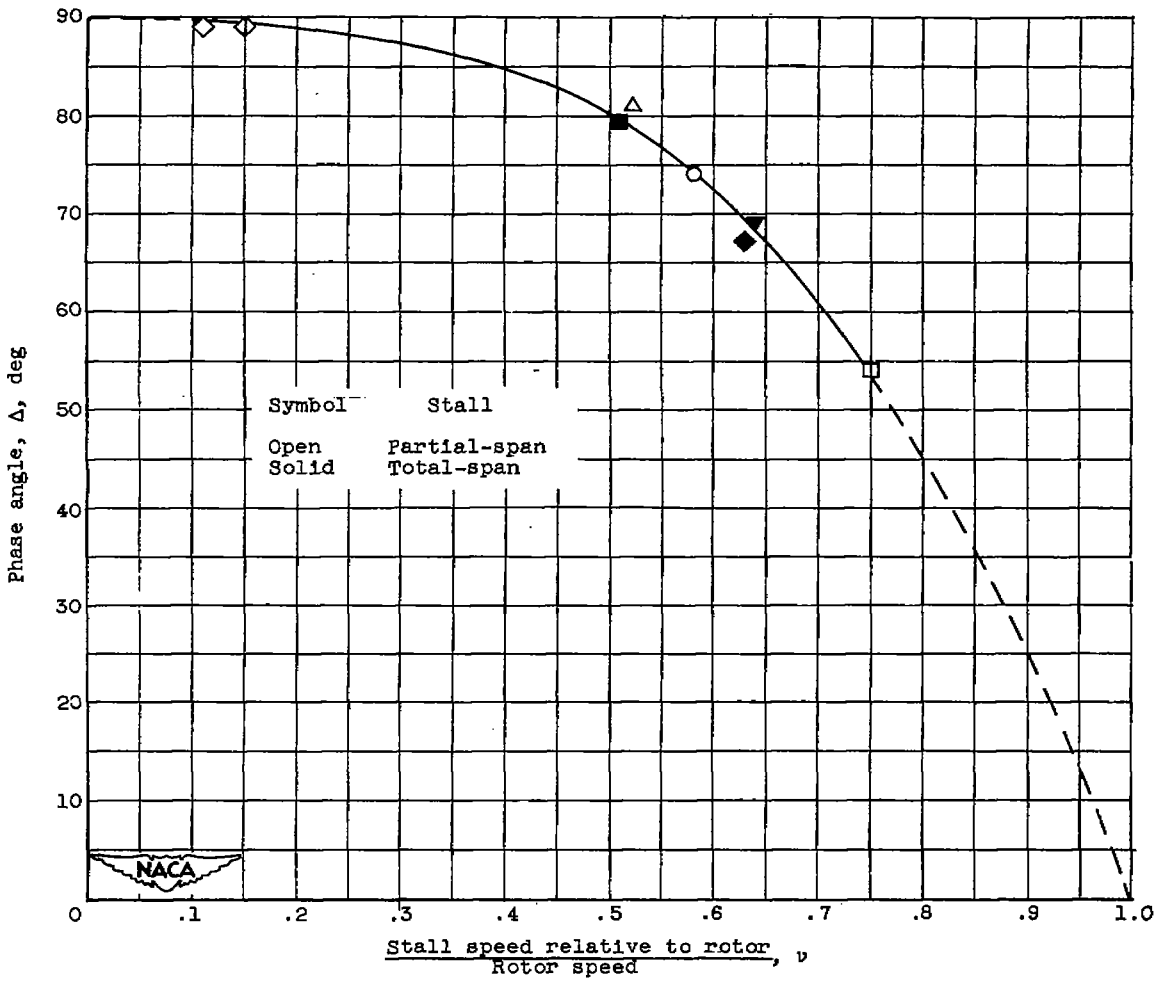

Figure 9. - Relation between stall rotational speed relative to rotor and phase angle.

[redacted]

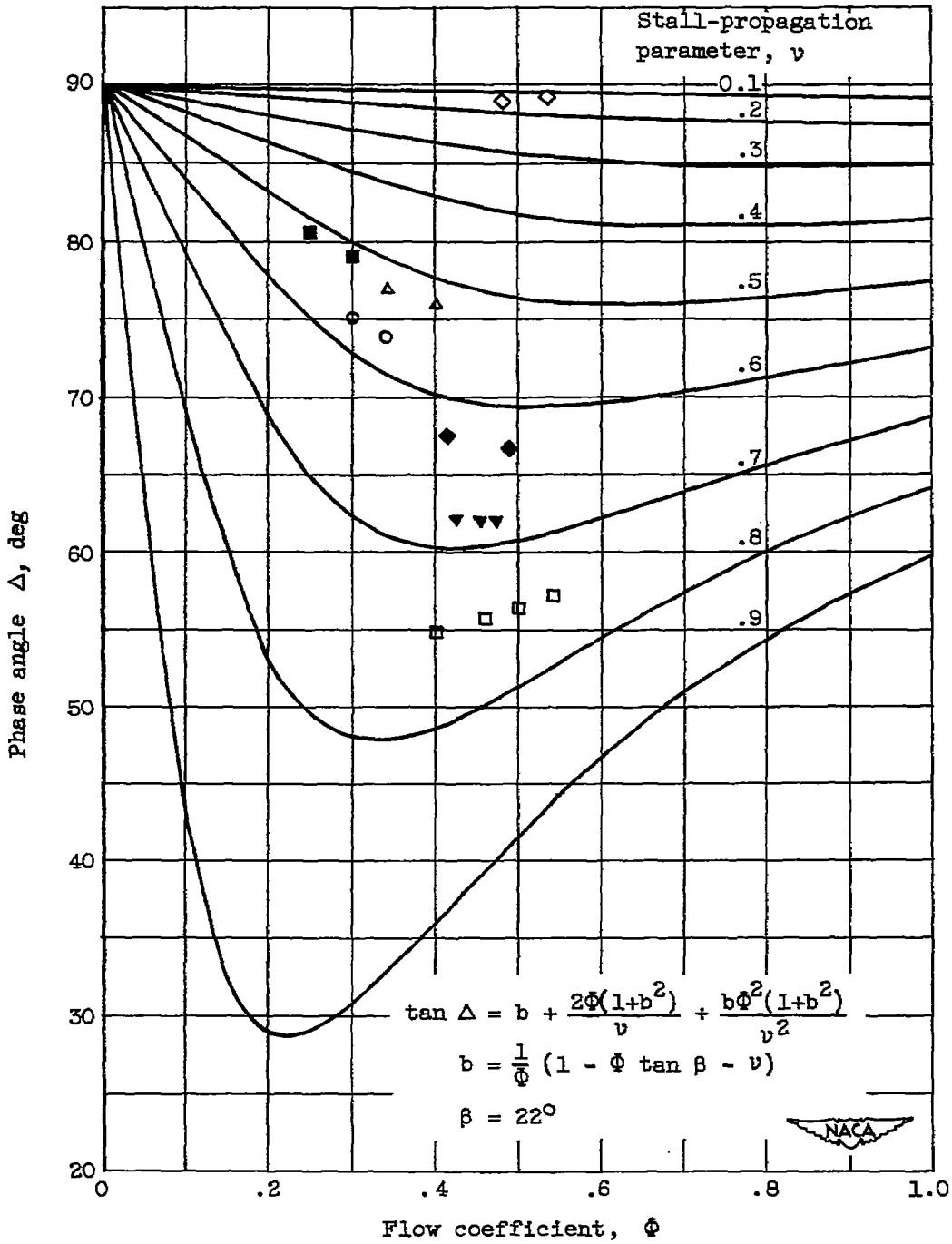

Figure 10. - Theoretical variation of phase angle with flow coefficient for constant values of stall-propagation parameter ν.

[redacted]

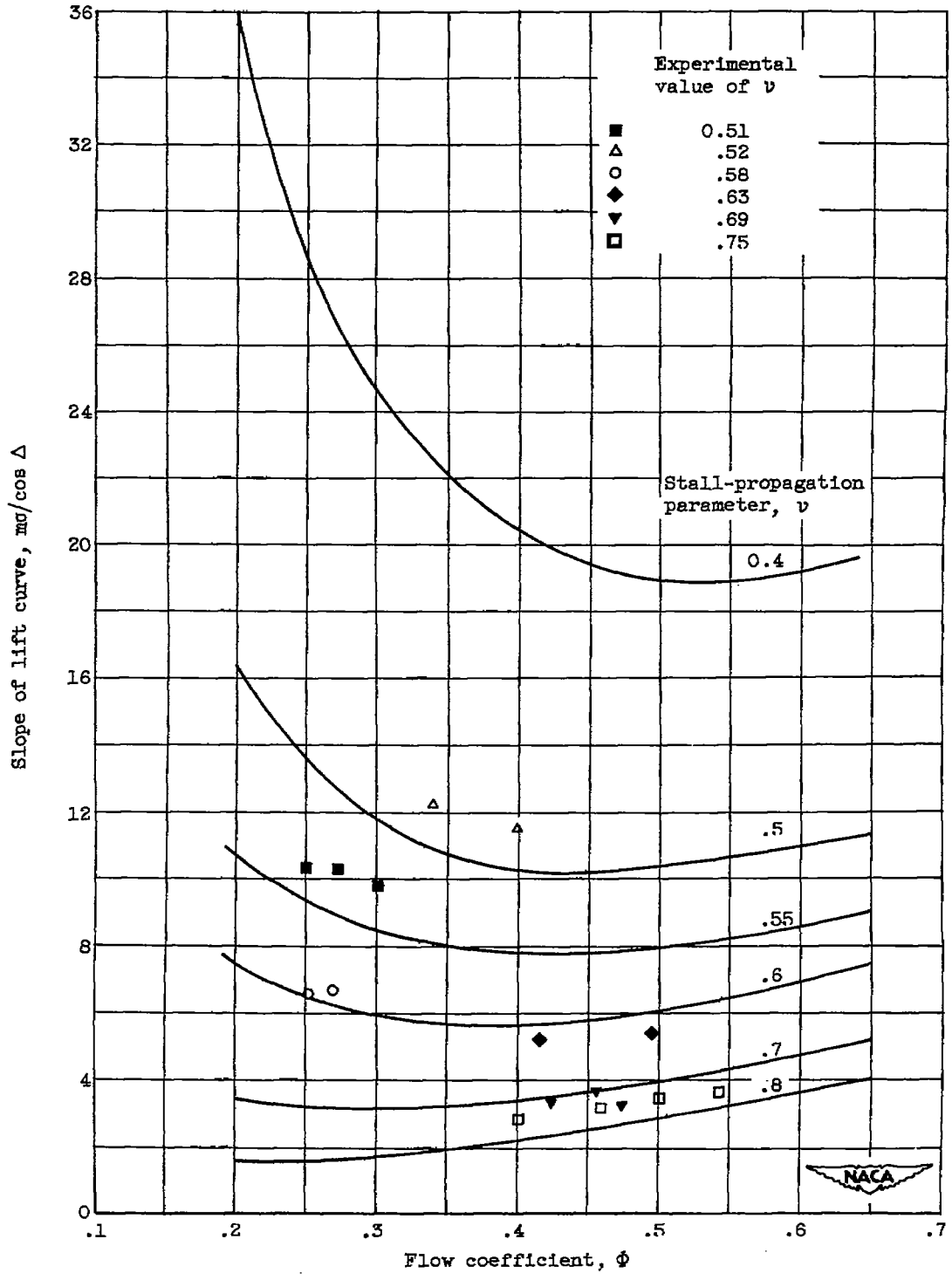

Figure 11. - Slope of lift curve as function of flow coefficient.

[redacted]L

[redacted]